Chapter 6

Synthesis, mechanical, polarization induced antibacterial and cellular response of 1393 BG–NKN composite

This chapter describes the effect of incorporation of varying amounts (0 – 30 vol. %) of piezoelectric NKN secondary phase in 1393 BG (53 wt. % SiO_2, 6 wt. % Na_2O, 12 wt. % K_2O, 5 wt. % MgO, 20 wt. % CaO, 4 wt. % P_2O_5) on mechanical, antibacterial and cellular response. The chapter begins with phase evolution of the sintered monolithic as well as composite samples. Various mechanical properties such as, hardness, fracture toughness, flexural and compressive strengths were evaluated for optimally sintered composite samples and a comparison has been made with those of the natural bone. In addition to the consequences of secondary phase content, this chapter also discusses the effect of polarization of the developed composites on antibacterial response. Towards the end, the combined effect of surface polarization as well as electric field treatment on cellular (MG 63 cells) response, while cultured on the developed composites.

6.1 Phase evolution

Fig. 6.1 shows the X-Ray diffraction (XRD) patterns of the sintered pure 1393 BG, NKN and 1393 BG–(10-30) NKN composites. The indexing was done for intense peaks. XRD pattern of sintered monolithic 1393 BG samples confirms the formation of hexagonal crystalline phase of 1393 BG (# 45-0136)XRD pattern of NKN also confirms the formation of phase pure $Na_{0.5}K_{0.5}NbO_3$ (#77-0038). XRD patterns of the 1393 BG–(10-30) NKN composites suggest that there is no dissociation of 1393 BG and NKN phases as well as any reaction between 1393 BG and NKN phases has not taken place [Fig.6.1].

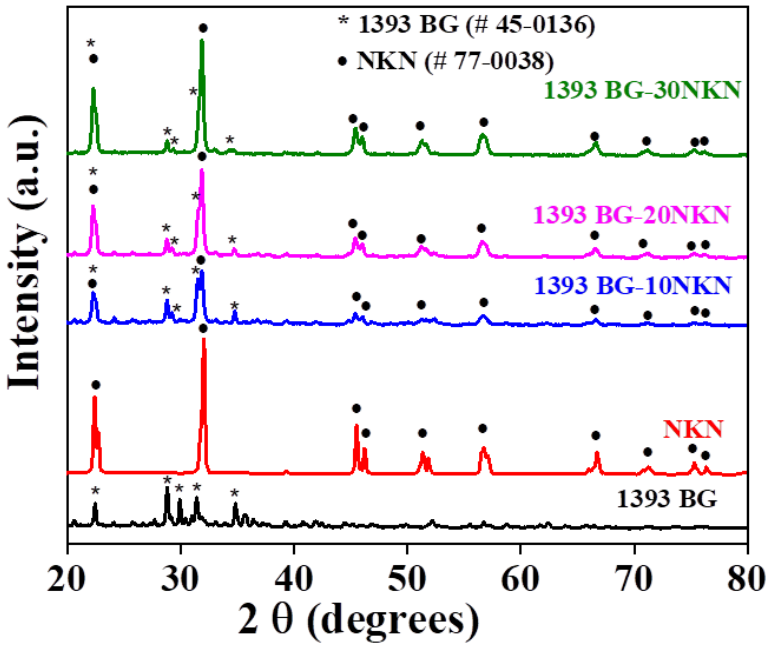

Fig. 6.1 X-Ray diffraction patterns for sintered (a) 1393 BG, (b) NKN, (c) 1393 BG - 10 NKN, (d) 1393 BG - 20 NKN and (e) 1393 BG - 30 NKN composite samples.

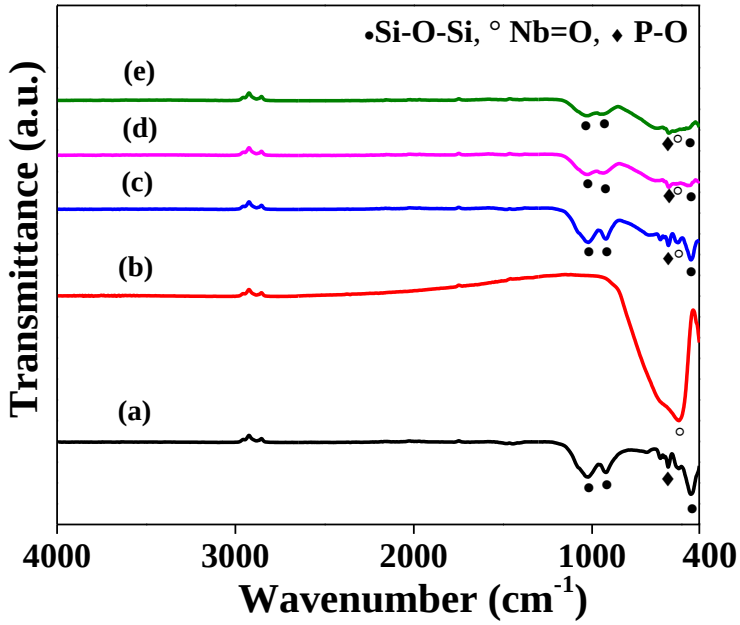

Fig. 6.2 Fourier transform infra-red (FTIR) spectra for sintered (a) 1393 BG, (b) NKN, (c) 1393 BG - 10 NKN, (d) 1393 BG - 20 NKN and (e) 1393 BG - 30 NKN composite samples.

Fig. 6.2 shows the FTIR analyses of the 1393 BG sample. FTIR spectrum reveals the characteristic vibrational bands of 1393 BG at ~ 450 cm^{-1}, 939 cm^{-1} and 1040 cm^{-1},which correspond to Si-O-Si bonding [1]. The characteristic band at ~574 cm^{-1} is associated with P-O bands [Fig.6.2].FTIR spectra of NKN reveal the presence of the Nb-O octahedron peak at 524 cm^{-1}[1]. The functional groups Si-O-Si, P-O and Nb-O present at their respective wave numbers without any deviation. Overall, the FTIR spectra of 1393 BG - NKN composites corroborate well with those of the XRD results.

6.2 Mechanical properties

6.2.1 Hardness and fracture toughness

The densification of the sintered 1393 BG and 1393 BG – (10 - 30) NKN composite samples were measured to be 95 ± 0.35, 96 ± 0.2, 97 ± 0.2 and 98.2 ± 0.25 % with respect to the their theoretical densities [Fig. 6.3]. Fig. 6.4(a) shows the variation of Vickers hardness as well as fracture toughness for 1393 BG – x NKN (x = 0 - 30 vol. %) composites. The hardness values of pure 1393 BG and 1393 BG – (10 - 30) NKN composites were obtained to be (3± 0.11), (3.76± 0.32), (4.42± 0.38) and (6.47 ± 0.22) GPa, respectively. 1393 BG – 30 NKN composite exhibits the maximum hardness value (almost more than 2 times of monolithic 1393 BG), which can be associated with the highest densification among all the composites.

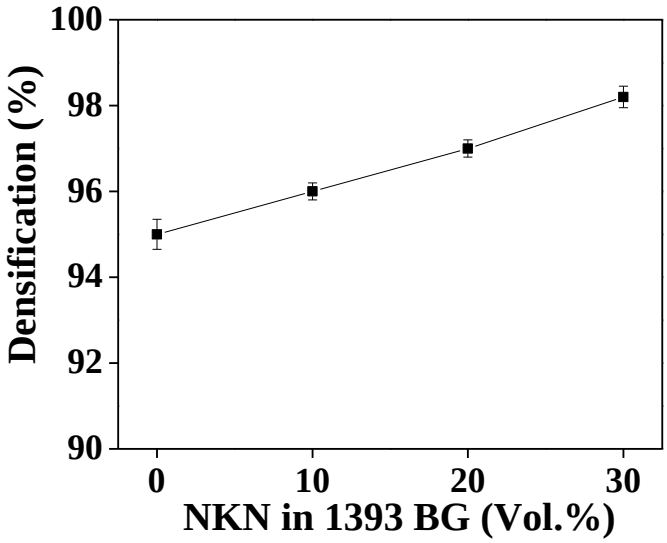

Fig.6.3. Densification behavior of 1393 BG and 1393 BG – (10 – 30 NKN).

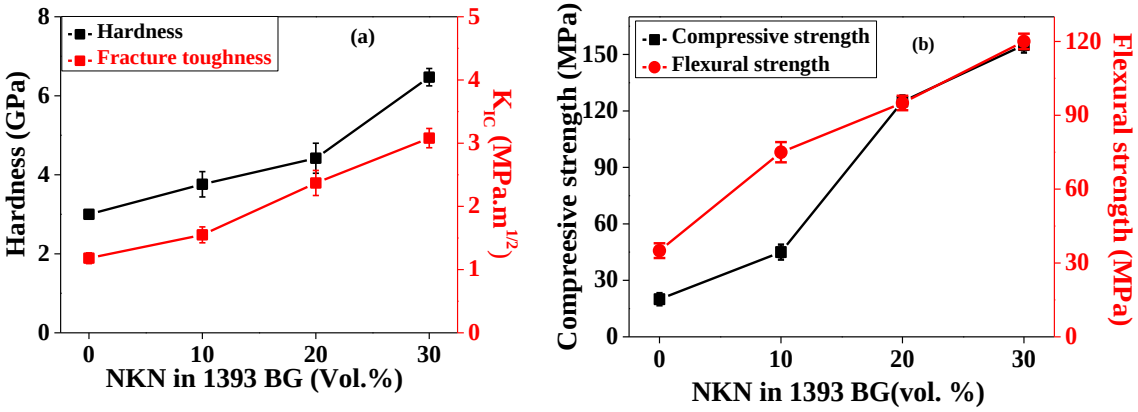

Fig.6.4. Variation of mechanical properties of 1393 BG with addition of NKN (a) Hardness and fracture toughness, (b) Compressive strength and Flexural strength

The indentation fracture toughness of monolithic 1393 BG and 1393 BG – (10 - 30) NKN composites were evaluated to be 1.18 ± 0.09, 1.55 ± 0.13, 2.37 ± 0.20 and 3.08 ± 0.15 MPa.m$^{1/2}$, respectively. The fracture toughness of 1393 BG – 30 NKN composite exhibits the maximum fracture toughness which is almost 2.6 times than monolithic 1393 BG. The piezoelectric toughening i.e., energy dissipation and domain switching has been suggested to provide additional toughening in such piezoelectric composite systems [2]. It has been reported that when a crack approaches the piezoelectric secondary phase in the

matrix, some part of crack energy is dissipated for the dipole alignment in a particular direction due to piezoelectricity. As a result, the energy required to propagate the crack decreases and consequently, the fracture toughness increases [3]. The mechanical load changes the domain alignment by 90° (maximum) whereas, the electric field changes the domain alignment by 180° [4].

6.2.2 Compressive and flexural strength

Fig. 6.4 (b) demonstrates the variation of compressive and flexural strengths of 1393 BG with the incorporation of piezoelectric NKN secondary phase. The compressive strength of the sintered monolithic 1393 BG and 1393 BG – (10 - 30) NKN composites were calculated to be20 ± 3.25, 45 ± 4, 125 ± 3.25 and 155 ± 4 MPa, respectively [Fig. 6.4 (b)]. The addition of piezoelectric NKN secondary phase in 1393 BG significantly enhances the compressive strength. The maximum compressive strength (155.15 ± 4 MPa) was calculated for 1393 BG - 30 NKN composite which is almost 8 times to the monolithic 1393 BG. The flexural strength of the sintered 1393 BG and 1393 BG – (10 - 30) NKN composite samples was obtained to be 35 ± 3, 75 ± 4.1, 95 ± 2.95 and 120 ± 3.15 MPa, respectively. The maximum flexural strength was obtained for 1393 BG - 30 NKN composite which is almost 3.5 times to that of monolithic 1393 BG [Fig. 6.4 (b)].The variation of flexural strength of 1393 BG with incorporation of NKN secondary phase is due to additional strengthening mechanism. The piezoelectric secondary phases dissipate the crack energy by their domain switching and consequently strengthen the material. As far as the compressive strength is concern, it is well known that the ceramics have higher compressive strength. The addition of NKN secondary phase further enhances by producing more grain boundaries and hinders the dislocation movement which consequently, provides additional strength [5,6].

Overall, it is observed that the addition of piezoelectric NKN secondary phase in1393 BG enhances the hardness, fracture toughness, compressive strength and flexural strength significantly.

6.3 Antibacterial behavior

6.3.1 MTT assay

Fig. 6.5 illustrates the antibacterial response of unpolarized and polarized monolithic 1393 BG and 1393 BG – (10 - 30) NKN composite system against gram positive *(S. aureus)* [Fig. 6.5 (a)] and gram negative *(E. coli)* bacteria [Fig. 6.5 (b)]. It is observed that the mean optical density for both, the bacterial cells decreases with addition of the piezoelectric NKN as the secondary phase in 1393 BG [Fig. 6.5]. Statistical analyses reveal the significant difference in mean optical density of uncharged, positively and negatively charged 1393 BG – (10 - 30) NKN composites than monolithic 1393 BG. Statistically significant reduction in the mean optical density of bacterial cells on unpolarized and polarized 1393 BG - (10 - 30) NKN composites are observed with respect to unpolarized monolithic 1393 BG [represented as * in Fig. 6.5 (a)].

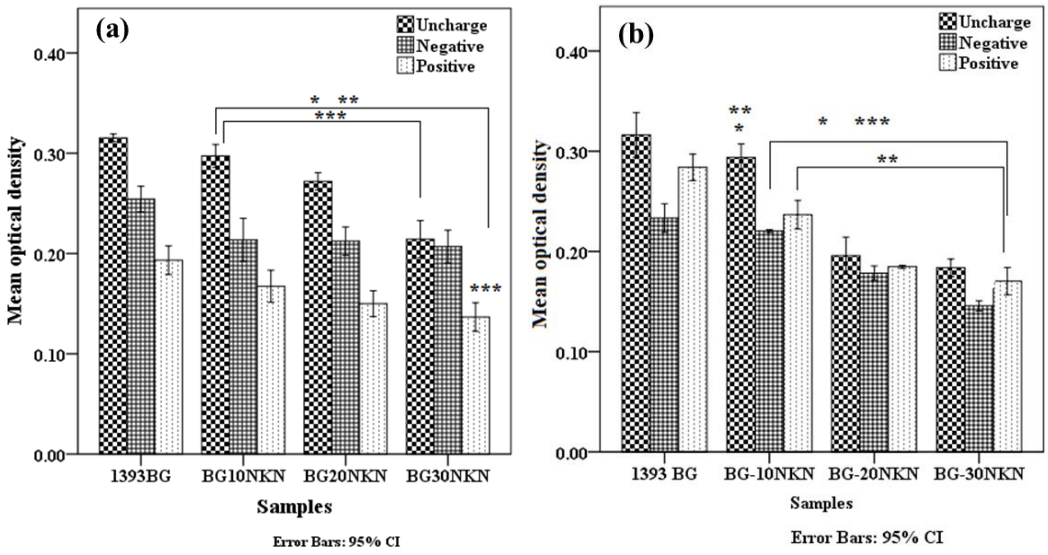

Fig. 6.5. Polarization induced antibacterial response of 1393 BG, 1393 BG - 10 NKN, 1393 BG - 20 NKN, 1393 BG - 30 NKN composites for (a) gram positive (S. aureus) and (b) gram negative (E. coli) bacteria. Asterisk (*), (**) and (***) marks represent the significant difference in optical density of bacterial cells for the uncharged, negatively and positively charged composite samples at $p < 0.05$, with respect to the monolithic 1393 BG.

As far as the influence of polarization on antibacterial response is concerned, positively charged 1393 BG–(10 – 30) NKN composites significantly decreases the mean optical density of *S. aureus* bacteria except negatively charged 1393 BG – 30 NKN composites, as compared to the negatively and positively charged monolithic 1393 BG [represented as ** and ***, respectively, in Fig. 6.5 (a)]. Similarly, for gram negative (*E. coli*) bacteria, the optical density of cells on 1393 BG - (10 - 30) NKN composites, decreases with respect to those on uncharged 1393 BG [represented as * in Fig. 6.5 (b)]. Statistical analyses reveal that the mean optical density of *E. coli*, on negatively charged surfaces of 1393 BG - (10 - 30) NKN composites decreases significantly, except negatively charged 1393 BG – 10 NKN composite, with respect to negatively charged 1393 BG [represented as ** in Fig. 6.5 (b)]. A significant decrease in optical density is observed for 1393 BG –

(10 – 30) NKN composites except uncharged 1393 BG – 10 NKN with respect to the positively charged monolithic 1393 BG.

6.3.2 NBT assay

Fig. 6.6 demonstrates the superoxide production (in terms of absorbance at 595 nm) by bacterial cells, cultured on unpolarized and polarized (negatively and positively) 1393 BG, 1393 BG – (10 – 30) NKN composites for gram positive [Fig. 6.6 (a)] and gram negative [Fig. 6.6 (b)] bacterial cells. Statistically significant difference in superoxide production can be clearly seen for 1393 BG – NKN composites than monolithic 1393 BG. It is also been clear from statistical analysis that superoxide production enhanced on unpolarized and polarized 1393 BG - (10 - 30) NKN composite samples in comparison to unpolarized and polarized HA samples (represented *, ** and ***, respectively in Fig. 6.6). Besides this, the statistically significant difference in superoxide production has also been observed on positively polarized surface in comparison to unpolarized and negatively polarized surfaces, irrespective of composition and bacteria type. It has been reported earlier that electric field, created due to polarization induces the electrolysis of water, which leads to ROS generation.[7] Superoxide, a ROS, destabilizes Fe^{2+} ions by damaging iron– sulphur clusters in proteins. This iron reacts with hydrogen peroxide and generate hydroxyl radicals in the Fenton reaction ($Fe^{2+} + H_2O_2 \longrightarrow Fe^{3+} + HO^{\bullet} + OH^-$). These radicals damage DNA, lipids, and proteins of the bacterial cells [8].

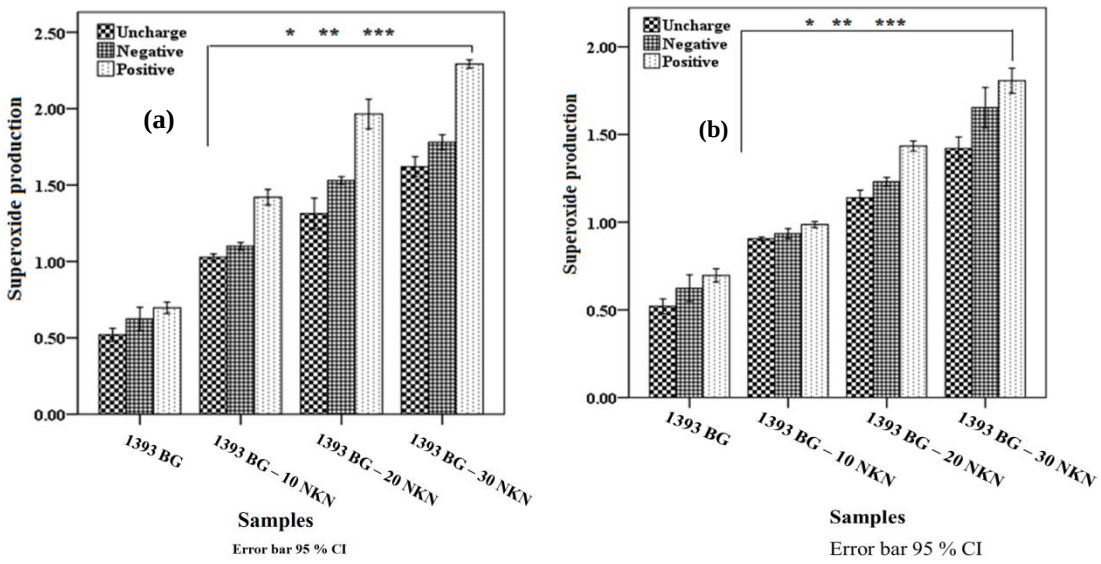

Fig. 6.6. Superoxide production (ROS generation) on monolithic 1393 BG, 1393 BG -10 NKN, 1393 BG - 20 NKN and 1393 BG-30 NKN composites for (a) gram positive (S. aureus) and (b) gram negative (E. coli) bacteria. Asterisk (*), (**) and (***) mark represent the significant difference in superoxide production by the bacterial cells for the uncharged, negatively and positively charged samples at $p < 0.05$, with respect to the monolithic 1393 BG.

6.3.3 Antibacterial ratio

S. aureus and *E. coli* bacterial cells, seeded on 1393 BG, 1393 BG – (10 – 30) NKNcomposite samples were incubated for 6-8 h at 37°C to allow cell adhesion. Then, the samples were washed gently 2-3 times to remove unattached bacterial cells. After that, the samples were transferred to new 24 well cell culture plate, filled with 1 ml of 1x PBS and ultrasonicated for 5 min to detach the bacterial cells from samples surface. This collected bacterial suspension were re-cultured into agar culture plate and incubated overnight at 37°C. Following this, the culture plates were observed for colony formation unit (CFU) and antibacterial rate was calculated using the formula [9],

[Antibacterial rate (%) = (CFU control−CFU experimental groups) / CFU control × 100%].

Figs. 6.7 (a) and (b) demonstrate the colony formation in agar cultured plate by *S. aureus* and *E. coli* bacterial cells.

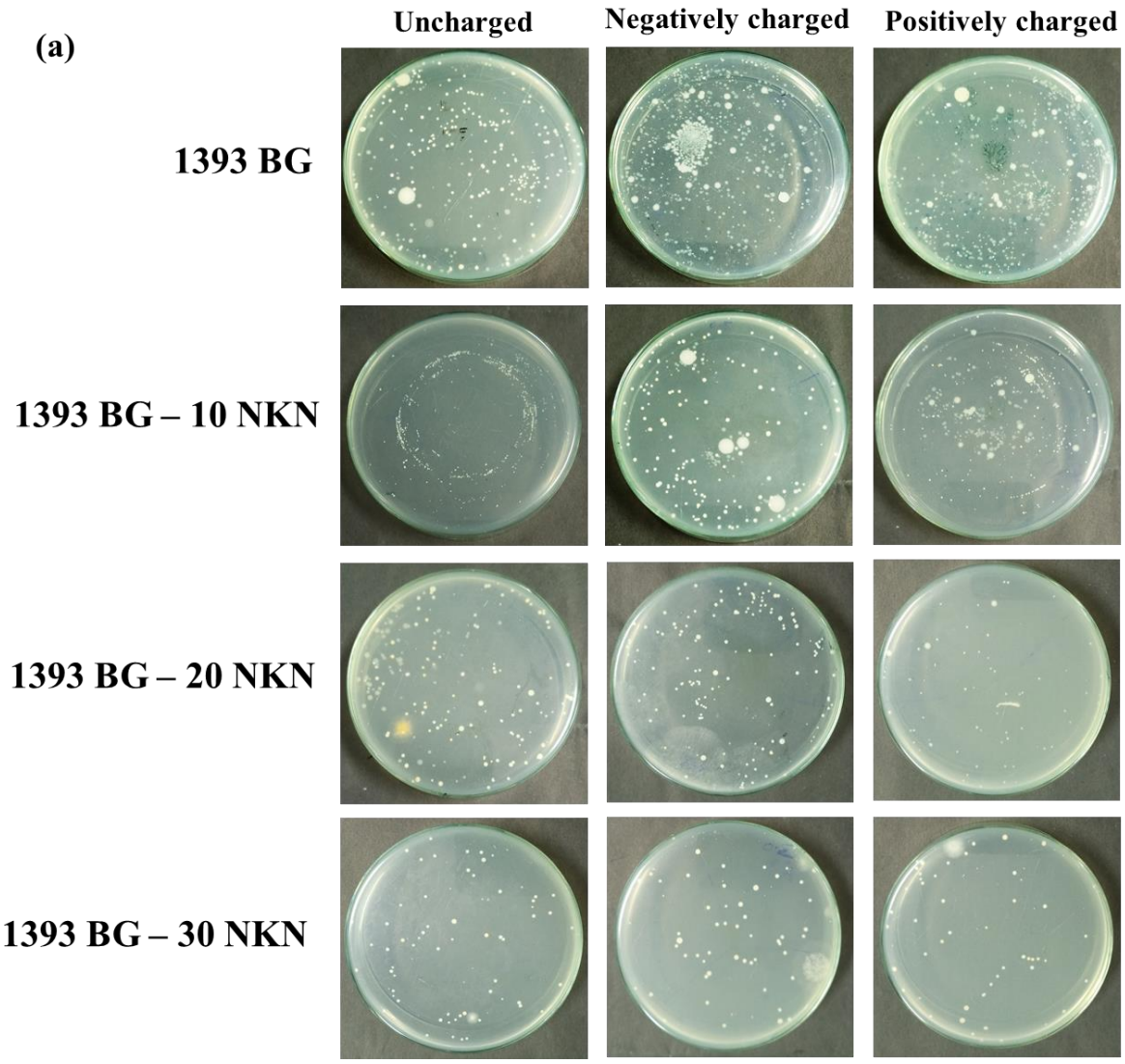

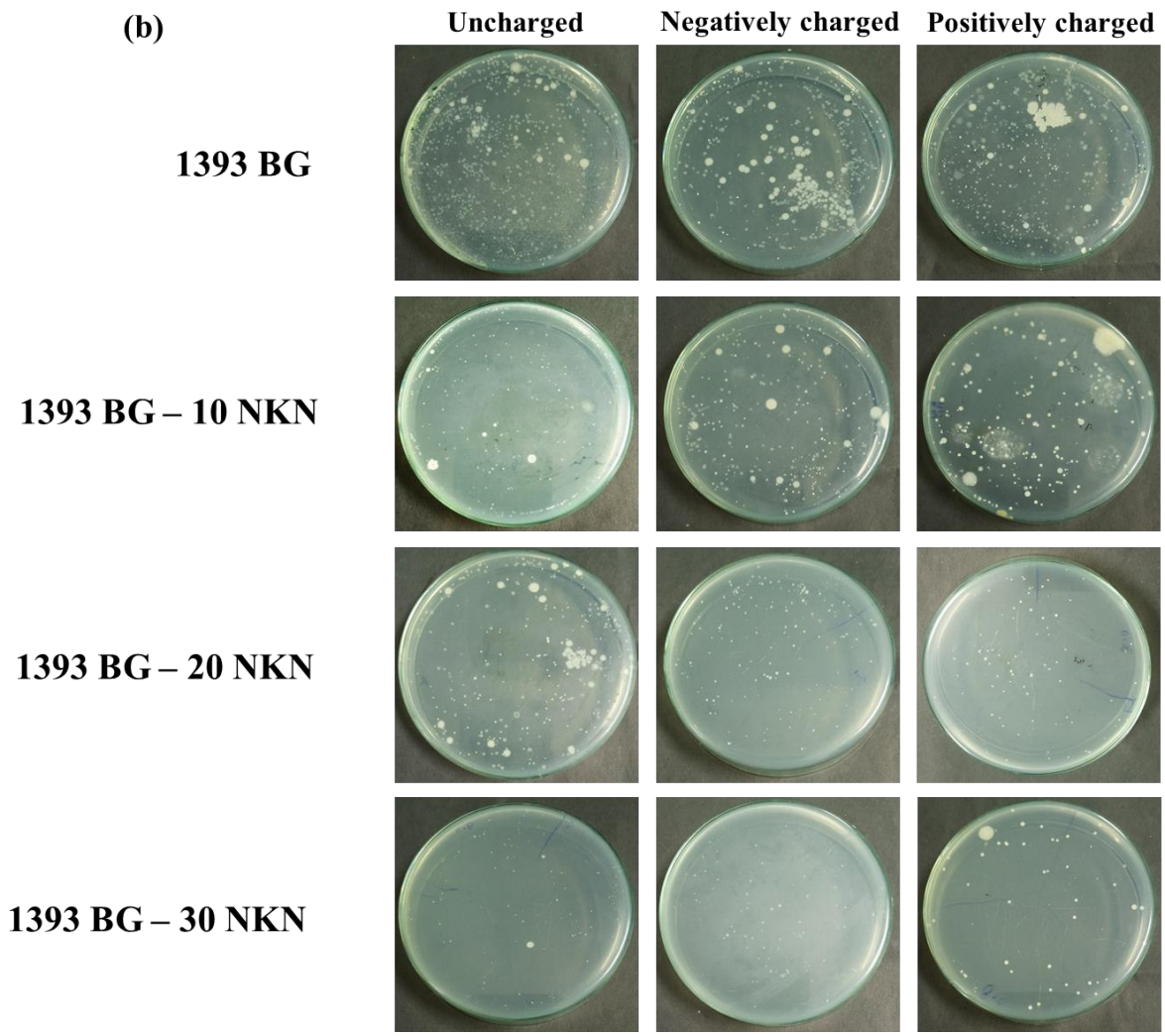

Fig. 6.7. Digital camera images, demonstrating the viable bacterial colonies of (a) S. aureus and (b) E. coli bacteria, cultured for 8 h on unpolarized and polarized 1393 BG, 1393 BG – 10 NKN, 1393 BG – 20 NKN and 1393 BG – 30 NKN composites.

Figs. 6.7 (a) and (b) represent the colonies of *S. aureus* and *E. coli* bacteria, cultured on unpolarized and polarized 1393 BG, 1393 BG – 10 NKN, 1393 BG – 20 NKN and 1393 BG – 30 NKN composites, respectively. It is clearly observed that the addition of piezoelectric NKN in 1393 BG reduces the bacterial growth. Among all the cultured samples, positively and negatively charged 1393 BG – 30 NKN composites is observed to exhibit best antibacterial response [Figs. 6.7 (a) and (b)].

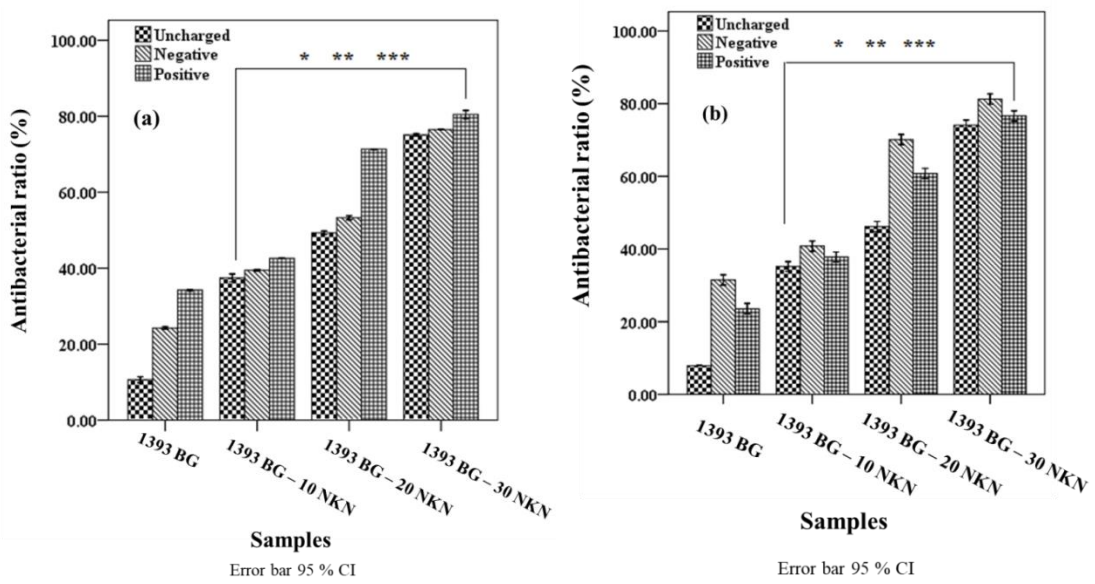

Fig.6.8. Antibacterial ratio for (a) gram positive (S. aureus) and (b) gram negative (E. coli) bacteria, cultured on monolithic 1393 BG, 1393 BG -10 NKN, 1393 BG-20 NKN and 1393 BG-30 NKN composites. Asterisk (*), (**) and (***) mark represent the significant difference of the uncharged, negatively and positively charged samples at p < 0.05, with respect to the monolithic HA.

Figs. 6.8 (a) and (b) represent the antibacterial response of 1393 BG – NKN samples in terms of antibacterial ratio. The antibacterial ratio of *S aureus* bacterial cells for positively polarized 1393 BG – 30 NKN composite surface is about 81%, which is more effective in comparison to negatively polarized 1393 BG – 30 NKN (76.52 %) and unpolarized 1393 BG – 30 NKN (75.22 %) composite. Since the samples were washed before seeding for CFU assay, it is also inferred that positively polarized surface counteract against bacterial adhesion i.e., demonstrate higher antibacterial rate. Addition of secondary phase also enhances the antibacterial response which is about 80.87 %, 76.52 % and 75.22 % for positively, negatively and unpolarized BG-30NKN composite, respectively, which is higher than BG – 10NKN (42.61 %, 39.57 %, and 37.83 %) and BG – 20NKN (71.30 %, 53.04 %, and 49.13%) composites. Similarly, the antibacterial ratio of *E. coli* bacterial cells for negatively polarized 1393 BG – 30 NKN composite surface is about 80.93 %

which is more effective in comparison to positively polarized 1393 BG – 30 NKN (76.28 %) and unpolarized 1393 BG – 30 NKN (74.42 %) composite. Since the samples were washed before seeding for CFU assay, it is also inferred that positively polarized surface counteract against bacterial adhesion on its surface i.e., higher antibacterial rate. Addition of secondary phase also enhances the antibacterial responses which is (80.93 %, 76.28 % and 74.42 %) for negatively, positively and unpolarized BG – 30NKN composites, respectively, which is higher than BG – 10 NKN (40.47 %, 38.13 % and 34.88 %) and BG – 20 NKN (69.76 %, 60.47 % and 46.50 %) composites. It is, therefore, clear that BG – 30NKN composite offer greater antibacterial capability. Overall, it can be suggested that the induced surface charge and increasing proportion of NKN can potentially increase the antibacterial rate.

A layer of lipopolysaccharides and peptidoglycan in outer cell membrane of gram negative and gram positive bacteria possess the negative charges [10,11]. Teichoic acids, embedded in peptidoglycan layer of gram- positive bacterial cell wall, are responsible for negative charge on the bacterial cell surface. The carboxylate and phosphate groups in teichoic acid contribute to the net negative charge [12]. It has been reported that bacterial cells can be repelled by negatively charged surface whereas, positively charged surfaces depolarize the cell membrane of bacterial cell which leads to cell death [13]. In addition, polarized surfaces increase the generation of reactive oxygen species (ROS) by the bacterial cells due to microelectrolysis [14]. ROS contains peroxides, superoxides, hydroxyl radical singlet oxygen, alpha oxygen etc. which are toxic in nature and damage the bacterial cells [15,16].

6.4 *In vitro* cytocomapatibity

6.4.1 Cell Viability

Fig. 6.9 demonstrates the MTT assay result for untreated and electric field (E-field) treated cells, cultured on 1393 BG and 1393 BG-30 NKN composite and incubated for 3, 5, and 7 days. It has been observed that unpolarized 1393 BG – 30 NKN composite shows the statistically significant difference in cell viability as compared to monolithic 1393 BG. The statistical significant difference in cell proliferation was observed for cells, cultured for 5 and 7 days in comparison to cells, incubated for 3 days, irrespective of sample type and E-field treatment. It has also been observed that negatively polarized surface promote cell proliferation in contrast to positively polarized and unpolarized surfaces, for both 1393 BG and 1393 BG – 30 NKN samples. For 7 days of incubation, it has been observed that negatively charged 1393 BG – 30 NKN composite shows the maximum cell viability in terms of optical density. Also, it has been found that negatively charged 1393 BG - 30 NKN composite exhibits higher cell viability in comparison to unpolarized and polarized pure 1393 BG for the same incubation period. In addition, external electric field further enhances the cell viability on negatively polarized surface. Thus, it is concluded that surface charge, in combination with external E-field, promote the cell growth and proliferation.

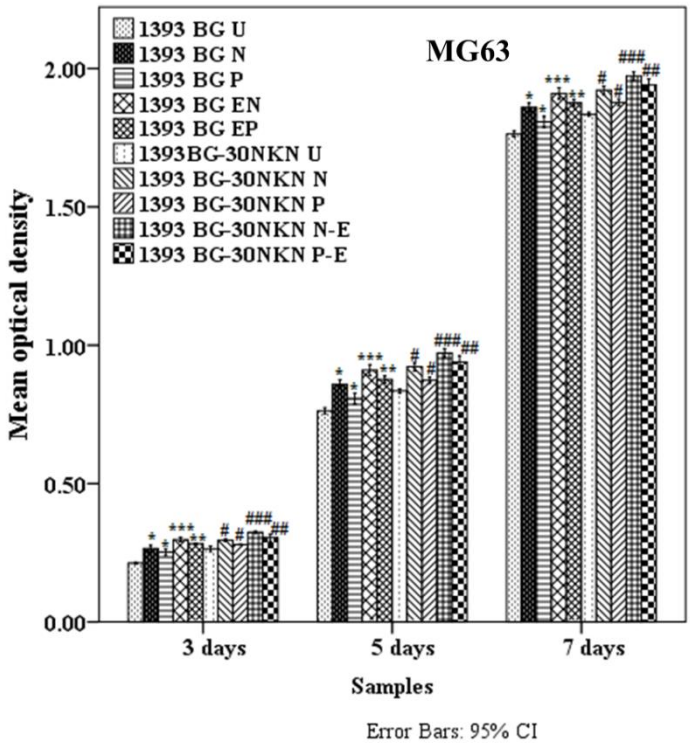

Fig.6.9.Time dependent cell viability of MG63 cells, cultured on unpolarized and polarized surfaces of 1393 BG and 1393 BG-30 NKN composites along with electric field treatment. (*) and (#) represent the statistically significant difference in optical density for negatively and positively charged 1393 BG and 1393 BG – 30 NKN composite with respect to uncharged 1393 BG and 1393 BG-30 NKN composite, (**) and (##) show the statistically significant difference in optical density for electric field treated positively charged 1393 BG and 1393 BG-30 NKN composite with respect to positively charged 1393 BG and 1393 BG-30 NKN composite and (***) and (###) show statistically significant difference in optical density for electric field treated negatively charged 1393 BG and 1393 BG-30 NKN composite with respect to negatively charged 1393 BG and 1393 BG-30 NKN composite.

6.4.2 Morphological Analysis

Fig. 6.10 shows the fluorescence images of untreated and electric field (E-field) treated MG-63 cells, cultured on unpolarized and polarized pure 1393 BG and 1393 BG – 30

NKN composites. The cell density is observed to be higher on negatively polarized surface in comparison to positively polarized and unpolarized surfaces. Further, the cell density is observed to be increased on electric field treated polarized samples in comparison to untreated samples. In addition, cells appear to be more dense and flattened on 1393 BG – 30 NKN composite in comparison to 1393 BG samples, irrespective of surface charge and electrical stimulation. It has been reported that, in addition to cell proliferation, polarized material surface also promotes early cell adhesion and spreading [17].

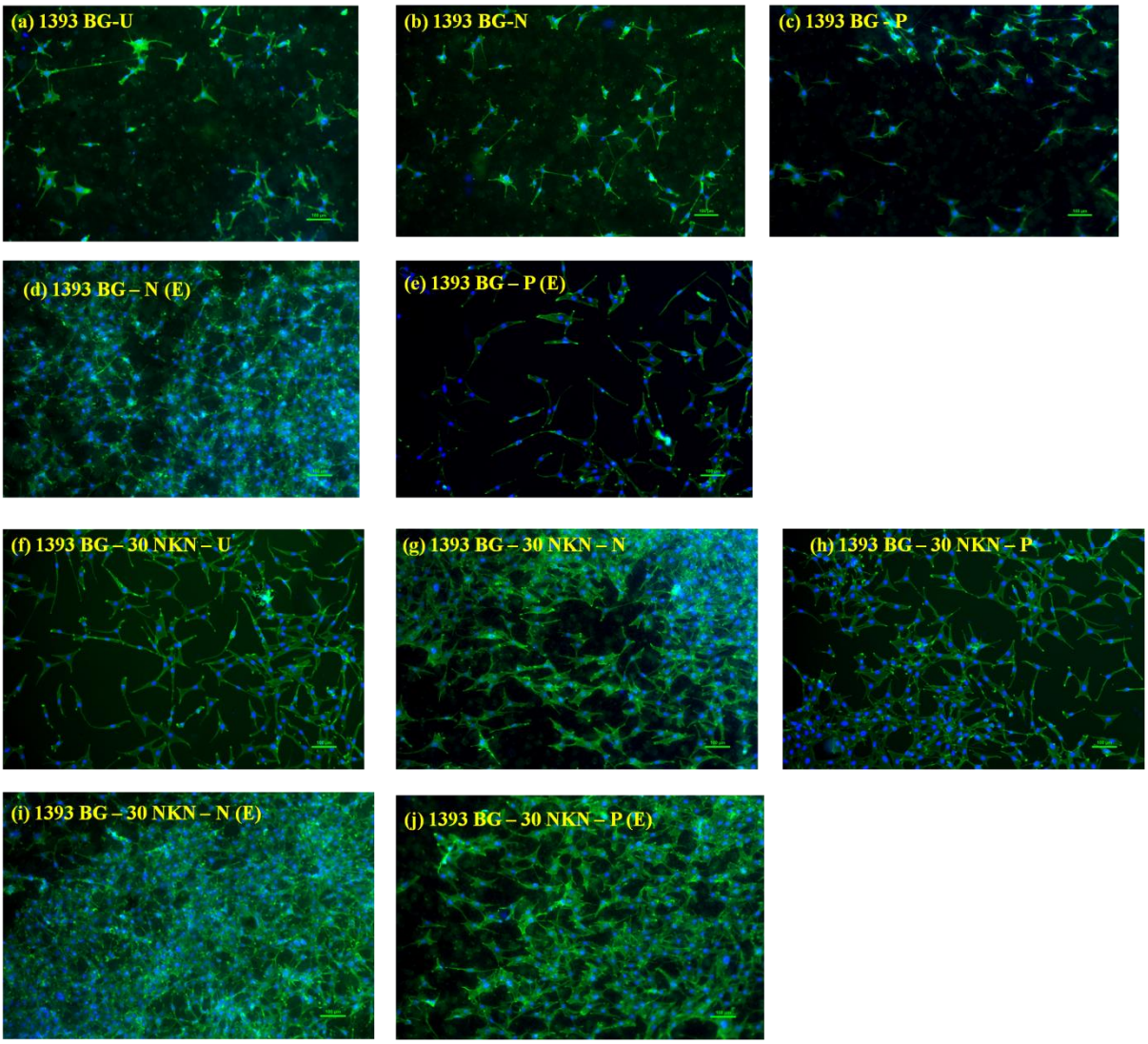

Fig. 6.10.Fluorescence images, demonstrating the morphology of MG63 cells, while cultured for 72 h on (a) uncharged 1393 BG, (b) negatively polarized 1393 BG, (c) positively polarized 1393 BG, (d) E-field treated negatively polarized 1393 BG, (e) E-field treated positively polarized 1393 BG (f) uncharged 1393 BG – 30 NKN composite, (g) negatively polarized 1393 BG – 30 NKN composite, (h) positively polarized 1393 BG – 30 NKN composite, (i) E-field treated negatively polarized 1393 BG – 30 NKN composite and (j) E-field treated positively polarized 1393 BG – 30 NKN composite. The E-field strength was 1 V/cm. The scale bars correspond to 100 μm.

It has been demonstrated by several researchers that polarization induced surface charge can enhance osteoblast cell proliferation and new bone formation [18 -23] It was also reported that the negatively polarized 1393 BGsurface shows higher osteobonding ability in comparison to positively polarized surface [24– 26]. Owing to electrostatic interaction, Ca^{2+}ions present in media were attracted towards negatively polarized1393 BG and promote the cellular functionality. In addition, external electrical stimulation further accelerates cell adhesion proliferation by opening the voltage gated Ca^{2+} channels which promote the intracellular Ca^{2+} influx that enhances the cell proliferation [27 - 31]. Thus, the activation of cell proliferation pathway as well as inhibition of apoptosis due to external electric field is another factor for higher osteoconductivity on electrically treated samples.

Overall, present study reveals that the addition of piezoelectric NKN secondary phase in 1393 BG improves the mechanical, electrical and dielectric behavior and antibacterial response as well as in vitro cytocompatibility of 1393 BG-NKN composite system. In addition, cell proliferation enhances further due to the combined effect of polarization and E – field treatment.

6.5 Closure

1393 BG - (10 - 30 vol. %) NKN composites were synthesized by solid state synthesis route with more than 96 % densification. The 1393 BG - 30 vol. % NKN exhibited the maximum Vickers hardness, fracture toughness, compressive and flexural strengths among the developed composites. The addition of piezoelectric NKN phase in BG improves the antibacterial behaviour of 1393 BG - NKN composite against *S. aureus* and *E. coli* bacterial cells. Statistical analyses suggest that positively and negatively charged surfaces of 1393 BG - NKN composite significantly decreases the viability of gram positive (*S. aureus*) and gram negative (*E. coli*) bacterial cells. Irrespective of piezoelectric phase, combined effect of electrostatic and dynamic pulsed electrical stimulation enhances the cell proliferation significantly for 1393 BG – 30 vol. % NKN composite. Overall, the incorporation of piezoelectric NKN in 1393 BG improves the mechanical and polarization induced antibacterial as well as accelerates cellular functionality by the combined action of electrostatic and dynamic pulsed electrical stimulation.

References

1. D.Q. Zhang, Z.C. Qin, X.Y. Yang, H.B. Zhu, M.S. Cao, "Study on synthesis and evolution of sodium potassium niobate ceramic powders by an oxalic acid-based sol–gel method," *Journal of Sol-Gel Science and Technology*. **57(1)** (2011) 31-35.

2. X.M. Chen, B. Yang, A new approach for toughening of ceramics, *Materials Letters* **33** (1997) 37–240.

3. Yang W, Zhu T. Switch-toughening of ferroelectrics subjected to electric fields. *Journal of the Mechanics and Physics of Solids* **46(2)** (1998) 291-311.

4. A. S. Verma, D. Kumar, A. K. Dubey, "A review of an innovative concept to increase the toughness of the ceramics by piezoelectric secondary phases," *Ceramics International* **44** (2018) 16119–16127.

5. T. E. Mitchell, K. P. D. Lagerlof, A. H. Heuer, "Dislocations in Ceramics," *Journal of Materials Science & Technology*. **1** (1985) 944-949.

6. D. Chen, M. E. Sixta, X. F. Zhang, L. C. DE Jonghe, R. O.Ritchie, "Role of the grain-boundary phase on the elevated-temperature strength, toughness, fatigue and creep resistance of silicon carbide sintered with al, b and c," *Acta materialia*. **48** (2000) 4599–4608.

7. E Serena, E Figallo, N Tandon, C Cannizzaro, S Gerecht, N Elvassore, G. Vunjak-Novakovic, "Electrical Stimulation of Human Embryonic Stem Cells: Cardiac Differentiation and the Generation of Reactive Oxygen Species". *Experimental Cell Research* **315 (20) (**2009) 3611–3619.

8. P. Belenky, , D. Ye Jonathan, C. BM Porter, N. R. Cohen, M. A. Lobritz, T. Ferrante, S. Jain. "Bactericidal antibiotics induce toxic metabolic perturbations that lead to cellular damage." *Cell reports* **13 (5)** (2015): 968-980.

9. B. Tao, Y. Deng, L. Song, W. Ma, Y. Qian, C. Lin, Z. Yuan, L. Lu, M. Chen, X. Yang, K. Cai, "BMP2-loaded titania nanotubes coating with pH-responsive multilayers forbacterial infections inhibition and osteogenic activity improvement, Colloids and Surfaces B:" *Biointerfaces* **177** (2019) 242–252

10. M Bellantone, NJ Coleman , L L Hench , Bacteriostatic action of a novel four-component bioactive glass, *Journal of Biomedical Materials Research.* **51(3) (**2000) 484-90.

11. E. Kłodzinska, M. Szumski, E. Dziubakiewicz, K Hrynkiewicz, E Skwarek, W Janusz, B. Buszewsk, "Effect of zeta potential value on bacterial behavior during electrophoretic separation," *Electrophoresis* **31** (2010) 1590–1596.

12. Y. Liu, R. Qin, SAJ Zaat, E. Breukink, M. Heger, "Antibacterial photodynamic therapy: overview of a promising approach to fight antibiotic-resistant bacterial infections" *Journal of Clinical and Translational Research* **1(3)** (2015) 140-167.

13. G. Harkes, J. Feijen and J..Dankert, "Adhesion of Escherichia coli on to a series of poly (methacrylates) differing in charge and hydrophobicity," *Biomaterials*, **12**, (1991), 853-860.

14. G. Tan, S. Wang, Y. Zhu, L. Zhou, P. Yu, X. Wang, T. He, J. Chen, C. Mao, C. Ning, "Surface-selective preferential production of reactive oxygen species on piezoelectric ceramics for bacterial killing." *ACS applied materials & interfaces* **8 (37)** (2016) 24306–24309.

15. M.P. Murphy, A. Holmgren, N.G. Larsson, B. Halliwell, C.J. Chang, B. Kalyanaraman, S.G. Rhee, P.J. Thornalley, L. Partridge, D. Gems, T. Nyström, "Unraveling the biological roles of reactive oxygen species," *Cell metabolism*, (4), **13** (2011) 361-366.

16. X.Q. Chen, X.Z. Tian, I. Shin, J. Yoon, “Fluorescent and Luminescent Probes for Detection of Reactive Oxygen and Nitrogen Species,” *Chemical Society Reviews* (9), **40** (2011)4783−4804.

17. M Nakamura, A Nagai, A Hentunen, J Salonen, Y Sekijima, T Okura, K Hashimoto, Y Toda, H Monma, K. Yamashita, “Surface Electric Fields Increase Osteoblast Adhesion through Improved Wettability on Hydroxyapatite Electret..” *ACS applied materials & interfaces* **1(10)** (2009) 2181–2189.

18. D . Kumar , J.P. Gittings, I.G. Turner, C.R. Bowen, L.A. Hidalgo-Bastida, S.H. Cartmell, “Polarization of hydroxyapatite: Influence on osteoblast cell proliferation,” *Acta Biomaterialia,* **6** (2010)1549-1554.

19. S. Itoh, S. Nakamura, M. Nakamura, K. Shinomiyaa, K. Yamashita, “Enhanced bone ingrowth into hydroxyapatite with interconnected pores by electrical polarization,” *Biomaterials,* **27** (2006) 5572-5579.

20. S. Nakamura, T. Kobayashi, K. Yamashita, “Extended bioactivity in the proximity of hydroxyapatite ceramic surfaces induced by polarization charges,” *Journal of Biomedical Materials Research* **61**(2002)593-599.

21.S. Itoh, S. Nakamura, T. Kobayashi, K. Shinomiya, K. Yamashita, “Effect of electrical polarization of hydroxyapatite ceramics on new bone formation,” *Calcified Tissue International* **78**(2006)133-42.

22. S. Itoh, S. Nakamura, M. Nakamura, K. Shinomiya, K. Yamashita, “Enhanced bone regeneration by electrical polarization of hydroxyapatite,” *Artif Organs,* **3** (2006) 863-9..

23. S. Itoh, S. Nakamura, M. Nakamura, K. Shinomiyaa, K. Yamashita, “Enhanced bone ingrowth into hydroxyapatite with interconnected pores by electrical polarization,” *Biomaterials,* **27** (2006) 5572-5579.

24. T. Kobayashi, S. Nakamura, K. Yamashita, “Enhanced osteobonding by negative surface charges of electrically polarized hydroxyapatite,” *Journal of Biomedical Materials Research*, **57** (2001)477-484.

25. N.C. Teng, S. Nakamura, Y. Takagi, Y. Yamashita, M. Ohgaki, K. Yamashita, “A new approach to enhancement of bone formation using electrically polarized hydroxyapatite,” *Journal of Dental Research*, **80** (2001) 1925-1292.

26. S. Nakamura, T. Kobayashi, K. Yamashita, “Numerical osteobonding evaluation of electrically polarized hydroxyapatite ceramics,” *Journal of Biomedical Materials Research A*, **68** (2004) 90-94.

27. A.K. Dubey, S.D. Gupta, B. Basu, “Optimization of electrical stimulation parameters for enhanced cell proliferation on biomaterial surfaces,” *Journal of Biomedical Materials Research Part B: Applied Biomaterial*, **8B** (2011) 18-29.

28. A. K. Dubey, B. Basu. Pulsed electrical stimulation and surface charge induced cell growth on multistage spark plasma sintered Hydroxyapatite-Barium Titanate piezobiocomposite *Journal of the American Ceramic Society*, **97 [2]** (2014) 481–489.

29. J. Tong, L. Sun, B. Zhu, Y. Fan, X. Ma, L. Yu, J. Zhang, “Pulsed electromagnetic fields promote the proliferation and differentiation of osteoblasts by reinforcing intracellular calcium transients,” *Bioelectromagnetics*, **38** (2017) 541-549.

30. M.Zhai, D. Jing, S. Tong, Y. Wu, P. Wang, Z. Zeng, G. Shen, X. Wang, Q. Xu, E. Luo, “Pulsed electromagnetic fields promote in-vitro osteoblastogenesis through aWnt/b-Catenin signaling-associated mechanism,” *Bioelectromagnetics*, **37** (2016) 152-162.

31. P. Zhou, F. He, Y. Han, B. Liu, S. Wei, “Nanosecond pulsed electric field induces calcium mobilization in osteoblasts,” *Bioelectrochemistry*, **124** (2018) 7-12.